

# The formation of C-shocks: structure and signatures

Michael D. Smith<sup>1</sup> and Mordecai-Mark Mac Low<sup>2</sup>

<sup>1</sup>Astronomisches Institut der Universität Würzburg, Am Hubland, D-97074 Würzburg, Germany

<sup>2</sup>Max-Planck-Institut für Astronomie, Königstuhl 17, D-69117 Heidelberg, Germany  
(smith@astro.uni-wuerzburg.de, mordecai@mpia-hd.mpg.de)

Received 28 March 1997 / Accepted 30 April 1997

**Abstract.** Shock waves in molecular clouds should evolve into continuous or C-type structures due to the magnetic field and ion-neutral friction. We here determine whether and how this is achieved through plane-parallel numerical simulations using an extended version of ZEUS. We first describe and test the adapted code against analytical results, laying the necessary foundations for subsequent works on supersonic ambipolar diffusion, including C-type jets and shock instability.

The evolution away from jump shocks toward the numerous steady C-shock sub-types is then investigated. The evolution passes through four stages, which possess distinctive observational properties. The time scales and length scales cover broad ranges. Specific results are included for shock types including switch, absorber, neutralised, oblique, transverse and intermediate. Only intermediate Type II shocks and ‘slow shocks’, including switch-off shocks, remain as J-type under the low ion levels assumed. Other shocks transform via a steadily growing neutral precursor to a diminishing jump. For neutralised shocks, this takes the form of an extended long-lived ramp.

Molecular hydrogen emission signatures are presented. After the jump speed has dropped to under  $25 \text{ km s}^{-1}$ , a non-dissociative jump section can dominate the spectra for a long period. This produces a high-excitation spectrum. Once the jump has further weakened, to  $< 8 \text{ km s}^{-1}$ , the fully developed ion front is responsible for brisk progress towards a constant C-type excitation. The time scale for emission-line variations is  $\sim (6/n_i) \text{ yr}$ , where  $n_i$  is the pre-shock ion number density.

**Key words:** shock waves – MHD – ISM: kinematics and dynamics – ISM: clouds – ISM: jets and outflows – ISM: lines and bands

---

## 1. Introduction

C-type shocks are frequently invoked to interpret the signatures of accelerated and excited gas in molecular clouds. These

*Send offprint requests to:* M.D. Smith

magnetically-mediated, two-fluid shocks are able to explain the survival of the molecules in shocks with velocities exceeding  $20 \text{ km s}^{-1}$  as well as the low excitation of observed spectra (e.g. the strong atomic fine-structure lines of oxygen and the low values of the 2-1 S(1)/1-0 S(1) ratio of molecular hydrogen). However, several basic questions on the existence of C-shocks remain to be answered. Under what conditions do steady-state C-shocks form? Is there sufficient time for the various C-shock configurations to be realized? Alternatively, how can we recognize an incomplete or proto-C-shock? Here, as part of a wider program to investigate supersonic ambipolar diffusion, we develop a numerical model and apply it to study the time-dependence of planar C-shock configurations.

A theory for steady C-shocks in molecular gas was constructed by Draine (1980) and applied by Draine, Roberge & Dalgarno (1983). The combination of low ion fraction, strong cooling, and significant (but not high) magnetic field results in a shock in which ion-neutral drag provides the viscosity, cooling keeps the gas supersonic and the field via the ions provides an extended cushioning layer which inhibits molecular dissociation (Draine & McKee 1993). Steady solutions for transverse-field C-shocks were further analysed by Chernoff (1987), Roberge & Draine (1990) and Smith & Brand (1990a). Smith, Brand & Moorhouse (1991) looked at the high-field ‘shock absorbers’. Wardle & Draine (1987) & Smith (1993a,b) presented a theory for oblique-field C-shocks, including the parallel-field C-switches. Flower, Pineau des Forêts & Hartquist (1985) considered the chemical aspects of steady C-shocks, work which has developed into a theory for C-shock chemistry (see Flower et al 1996). Predictions for steady, planar C-shocks were presented, in addition, by Smith & Brand (1990b), Smith (1991, 1995) and Kaufman & Neufeld (1996a,b).

Are these steady-state predictions relevant? Time dependence can enter for two reasons: instability and evolution. A two-dimensional instability was discovered by Wardle (1990, 1991a,b). It has been numerically modeled by Toth (1994, 1995), and more extensively in recent papers by Stone (1997) and Mac Low & Smith (1997a,b). Conditions for stability are either (i) neutral Alfvén numbers  $M_a = v_s/v_a < 5$ , where  $v_s$  and  $v_a = B/(4\pi\rho_n)^{1/2}$  are the shock and Alfvén speeds, respectively, or (ii)

rapid recombination so that the ion fraction is fixed locally rather than via advection. However, it is not clear that steady state models will apply even in the absence of instability. This evolutionary question, which has not been examined before (Pineau des Forêts 1997), is the focus of this paper. We use one-dimensional (and therefore stable), time-dependent computations to predict the speed and character of changes in the structure of a proto-C-shock. We use this knowledge to predict emission line strengths, to identify proto-C-shocks, and distinguish these changes from those produced in an unstable C-shock, as evaluated by Neufeld & Stone (1997) and Mac Low & Smith (1997b).

Our attempt to evolve flow patterns from a sharply discontinuous J-shock to a C-shock under constant ionization conditions may not exactly correspond to a physical situation. Rather, we use these examples to envisage how a flow accommodates to changing conditions such as those caused by the start of a stellar outflow, the impact of a jet on a cloud, or a cloud-cloud collision. Our primary goal here is to obtain a deeper understanding of how molecular shocks behave dynamically. We do use an alternative initial condition, with a smooth transition following a hyperbolic tangent function, to test the dependence of our results on the assumption of an initially sharp discontinuity.

This paper also represents one step in our exploration of supersonic ambipolar diffusion. The original ZEUS ambipolar diffusion code of Mac Low et al (1995) has been extended to cover more general molecular cloud conditions, by including ion mass conservation as opposed to the earlier assumption of a fixed ion number density. Hence it is first necessary to test the behavior of the extended code against standard C-shock solutions (§2). The fluid remains as before isothermal. We thus concentrate on the dynamical aspects. The ‘cool C-shock approximation’ (Smith & Brand 1990a) allows us to extract quantitative predictions for temperature and line emission.

## 2. Framework

### 2.1. Numerical methods

For our numerical computations, we use a modified version of the ZEUS code<sup>1</sup> (Stone & Norman 1992a,b). Ambipolar diffusion was added to ZEUS by Mac Low et al. (1995), who described the basic interface with the ZEUS code. Summarizing, that work made four approximations: isothermality of ions, electrons and neutrals, no electron-ion drift, ion density dependent in power-law fashion on neutral density, and no ion inertia or pressure. This allowed us to neglect, respectively, the energy equation, Ohmic diffusion, and the equations of ion mass and momentum conservation. This approach has proved adequate for modelling protostellar disks in the absence of strong shocks. However, the flow of ions can be important in C-shocks, for example in the Wardle instability, which is driven by the flow of ions along buckling field lines in the shock front.

Neglect of ion inertia and pressure had allowed the replacement of the ion momentum conservation equation by an alge-

<sup>1</sup> Available for community use by registration with the Laboratory for Computational Astrophysics at lca@nasa.uiuc.edu

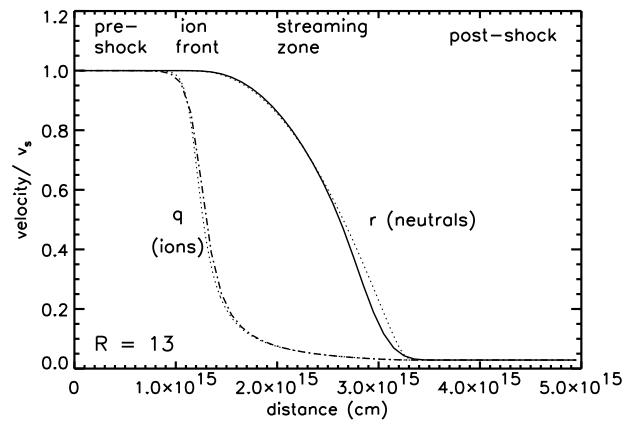


**Fig. 1.** The standard transverse-field C-shock reaches this steady state after  $5 \times 10^{10}$  s. The grid resolution  $R = \Delta x/L_n$ , where  $L_n$  is the neutral deceleration length, roughly corresponding to the shock thickness. Here we show a low-resolution run with  $R=13$  to emphasize the accuracy of the code. The dotted lines are the corresponding analytical solutions. The total compression  $S = 34.86$ .

braic equation expressing the balance between Lorentz forces and ion-neutral drag in determining the drift velocity between ions and neutrals. This approach is physically accurate and allows time steps determined by the equivalent of the Courant condition for ambipolar diffusion,  $\Delta t \leq \pi \gamma \rho_i \rho_n (\Delta x)^2 / |\mathbf{B}|^2$  (Mac Low et al. 1995). Both Tóth (1994) and we have found that this approach can be numerically unstable in the presence of steep velocity gradients as occur in C-shocks. However, in the one-dimensional models shown in this paper, this only occurs for switch shocks, and even there is not deadly to the computation, so we defer addressing this issue to our report on multi-dimensional models (Mac Low & Smith 1997b).

We treat the ions as a separate fluid in the code, using the standard ZEUS algorithms to update them. The equations we solve in the current version of the code are then the neutral and ion continuity equations, the neutral momentum equation, and the induction equation, as well as satisfying the zero-divergence criterion:

$$\partial \rho_n / \partial t = -\nabla \cdot (\rho_n \mathbf{v}_n) \quad (1)$$

$$\partial \rho_i / \partial t = -\nabla \cdot (\rho_i \mathbf{v}_i) \quad (2)$$

$$\rho_n (\partial \mathbf{v}_n / \partial t) = -\rho_n (\mathbf{v}_n \cdot \nabla) \mathbf{v}_n - \nabla P_n + \gamma \rho_i \rho_n (\mathbf{v}_i - \mathbf{v}_n) \quad (3)$$

$$(\partial \mathbf{B} / \partial t) = \nabla \times (\mathbf{v}_i \times \mathbf{B}) \quad (4)$$

$$\nabla \cdot \mathbf{B} = 0 \quad (5)$$

where the subscripts  $i$  and  $n$  refer to the ions and neutrals,  $\rho$ ,  $\mathbf{v}$ , and  $P$  are density, velocity and pressure for each fluid,  $\mathbf{B}$  is the magnetic field, and  $\gamma$  is the collisional coupling constant between the ions and neutrals.

We used the analytic jump conditions for a magnetized shock (e.g. Priest 1982) to set the values of the flow variables on both boundaries needed to hold the shock stationary on our grid. These are traditionally called ‘inflow’ boundary conditions, al-

**Table 1.** Initial and boundary conditions: the standard set.

neutral x-velocity	$v_n = rv_s$	50 km s <sup>-1</sup>	1.434 km s <sup>-1</sup>
ion x-velocity	$v_i = qv_s$	50 km s <sup>-1</sup>	1.434 km s <sup>-1</sup>
neutral y-velocity	$v_{ny} = r_y v_s$	0	0
ion y-velocity	$v_{iy} = q_y v_s$	0	0
density <sup>a</sup>	$n_H$	1 10 <sup>5</sup> cm <sup>-3</sup>	34.9 10 <sup>5</sup> cm <sup>-3</sup>
mag. field <sup>b</sup>	$B_y$	0.3430 mG	11.96 mG
ion abundance <sup>c</sup>	$\chi$	10 <sup>-6</sup>	10 <sup>-6</sup>

<sup>a</sup>This is the total hydrogen nuclei number density.

<sup>b</sup>The initial upstream Alfvén speed is 2 km s<sup>-1</sup>.

<sup>c</sup>The number of ions relative to  $n_H$ .

though on the downstream edge of our grid the flow is out rather than in.

## 2.2. Analytical background and parameter definitions

We begin by setting up a one-dimensional J-shock. We generated this solution from the standard shock jump conditions with magnetic field (e.g. Priest 1982). This is equivalent to assuming that the ion fraction was initially high, forcing the ions and neutrals to move at identical velocity. Given the shock speed, Alfvén speed, temperature and field direction, we can define the downstream values in terms of the upstream values. The supersonic inflow and subsonic outflow boundary conditions are then set so that the shock front remains stationary on the computational grid. Note that the shock front thus begins as a truly discontinuous jump rather than being spread out by numerical viscosity. We also use an initial condition with a smooth transition proportional to  $\tanh(x/L)$  for a given  $L$  to check the importance of the initial discontinuity.

We start with a standard set of initial conditions. This standard set represents a high Alfvén number shock ( $M_a = 25$ ) with a transverse magnetic field. In Table 1 we present all the physical conditions of the models shown in Figs. 1-4, apart from the sound speed of 100 cm s<sup>-1</sup>, helium abundance of 0.1, ion mass  $m_i = 10m_p$ , neutral mass  $m_n = 7m_p/3$  (assuming a fully molecular gas), and the coupling constant  $\gamma = \langle \sigma w \rangle / (m_i + m_n) = 9.21 \cdot 10^{13} \text{ cm}^3 \text{ s}^{-1} \text{ gm}^{-1}$ , corresponding to a fixed momentum transfer rate coefficient of  $\langle \sigma w \rangle = 1.9 \cdot 10^{-9} \text{ cm}^3 \text{ s}^{-1}$  (a rather uncertain parameter).

We then determine the corresponding steady-state C-shock solution. We describe this with the variables  $r(x, t) = v_n/v_s$ ,  $q(x, t) = v_i/v_s$  and the fixed temperature  $\tau = kT_n/(m_n v_s^2)$ . Hence  $r = q = 1$  upstream and the neutral and ion compression ratios are  $1/r$  and  $1/q$ , respectively. Assuming ion conservation and isothermality, the steady-state C-shock solution is then fully described by the total momentum equation

$$r + \frac{\tau}{r} + \frac{1}{2M_a^2 q^2} = 1 + \frac{1}{2M_a^2} \quad (6)$$

and the drag on the ions

$$L_n \frac{dq}{dx} = \frac{q^2(q-r)}{r} M_a \quad (7)$$

(Smith & Brand 1990a) where  $L_n = v_a/(\gamma\rho_i)$  is the neutral deceleration scale. For the ‘neutralised’ isothermal C-shock, in which the ion abundance is a constant, the momentum conservation condition is unaltered and the drag relation is then

$$L_n \frac{dq}{dx} = \frac{q^3(q-r)}{r} M_a. \quad (8)$$

Full steady-state solutions are derived by numerically solving these simple differential equations to any desired accuracy.

## 2.3. Scaling

Besides the length scale  $L_n$ , we define the ion deceleration scale  $L_i = L_n/M_a$ . A further scale defines the ion-neutral interaction region. In cool shocks, the maximum streaming speed occurs for  $q = 1/M_a^{2/3}$  (on putting  $t = 0$  in Eq. 6). The value of the maximum is  $(r-q)_{max} = 1 + M_a^{-2} - 3M_a^{-2/3}/2$ . It follows that high streaming speeds are maintained over a length scale  $L_{str} \sim L_n/M_a^{1/3}$ . Finally note that the length scale defined by Wardle (1990, 1991a,b) is  $L_{shk} = \sqrt{2} L_n$ . We define here what proves to be a better measure of the shock length for transverse shocks:  $L_{sm} = L_n/(r-q)_{max}$ . This enables low  $M_a$  shocks to be also included.

The time-dependent shock flow pattern is fully determined by four control parameters: the Alfvén number  $M_a$ , the Mach number  $M$ , the ion fraction and the initial field orientation. These are the only parameters which remain after scaling Eqs. (1–5) to the length scale  $L_n$  and the time scale  $t_{flow} = L_n/v_a$ . Therefore only one parameter is necessary to describe the whole class of transverse, low-ionisation, cold flows: a single flow simulation with a fixed Alfvén number is relevant to a wide range of conditions.

One must, however, ensure that the thermal pressure gradients remain small. This is easily achievable when close to the steady state since then the pressure gradient term  $\tau/r = c_s^2/(v_n v_s)$  is limited by the maximum compression ( $S \sim \sqrt{2}M_a$  for high  $M_a$ ) to the value  $(c_s^2/v_a^2)/S$ , where  $c_s$  is the sound speed. This is expected to be well below unity (and therefore ignorable) in strong shocks in molecular clouds. However, in time-dependent flows in general, depending on the imposed conditions, neutral speeds may approach zero and even an isothermal flow may possess high pressure gradients. The present simulations then require holding both the Mach and Alfvén numbers fixed.

Furthermore, the freedom to scale parameters while holding  $M_a$  fixed becomes physically invalid if the ion fraction depends on the other shock parameters. This limits the scaling regime to flows with ion-neutral streaming speeds less than  $\sim 42 \text{ km s}^{-1}$  to avoid runaway ionisation (Draine et al 1983, Smith & Brand 1990a).

The flow patterns presented below can thus be considered quite general provided the above rules are not violated. No scaling was attempted, however, when calculating the emission line properties, in order to avoid possible mis-matching when piecing together the results from separate models for the emission from the J-shock and the continuous section.

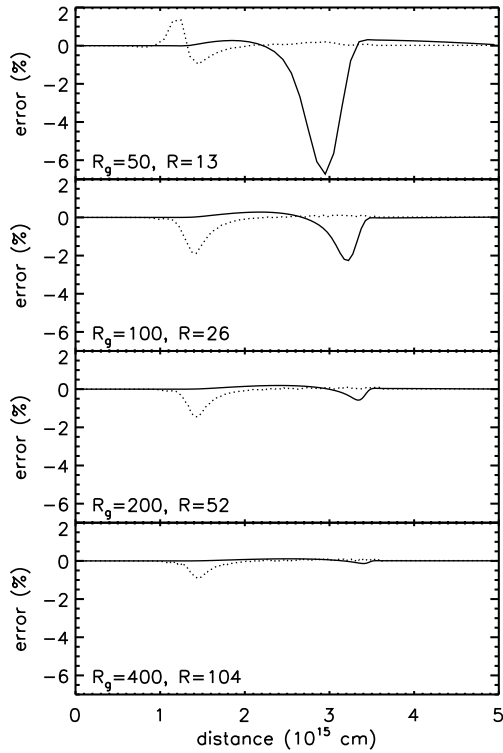


**Fig. 2.** The errors in the final configurations for simulations of the standard C-shock at the four indicated resolutions  $R = \Delta x/L_n$ . The number of zones in the full grid is given by  $R_g$ . The solid line is the momentum error and the dotted line is the streaming error.

#### 2.4. Test of accuracy

In our time-dependent computations, J-shocks indeed evolve to the analytical, steady C-shock solution to within our numerical accuracy. Fig. 1 presents the flow parameters at a time  $5 \cdot 10^{10}$  s. The length scale is  $L_n = 1.3 \cdot 10^{15}$  cm and the flow time scale is  $t_{flow} = L_n/v_a = 6.5 \cdot 10^9$  s. We find that it takes several flow time scales before the flow pattern finally settles down to the analytical steady state solution.

Fig. 2 demonstrates the dependence of the time-dependent solutions on the grid resolution. Even a grid size of  $R_g = 50$ , with the number of zones across the shock  $R = \Delta x/L_n = 13$ , is sufficient for dynamical purposes with the major error occurring in the final deceleration zone (at about  $3 \cdot 10^{15}$  cm). The error functions analysed in Fig. 2 are the momentum error (solid lines) given by

$$\epsilon_m(x) = \frac{r + 1/(2M_a^2 q^2)}{1 + 1/(2M_a^2)} \quad (9)$$

and the streaming error (dotted lines) given by

$$\epsilon_s(x) = [r_s - q_s] - r + q \quad (10)$$

where  $[r_s - q_s]$  is the analytical steady streaming solution. The expected second order convergence (Mac Low et al 1995) occurs.

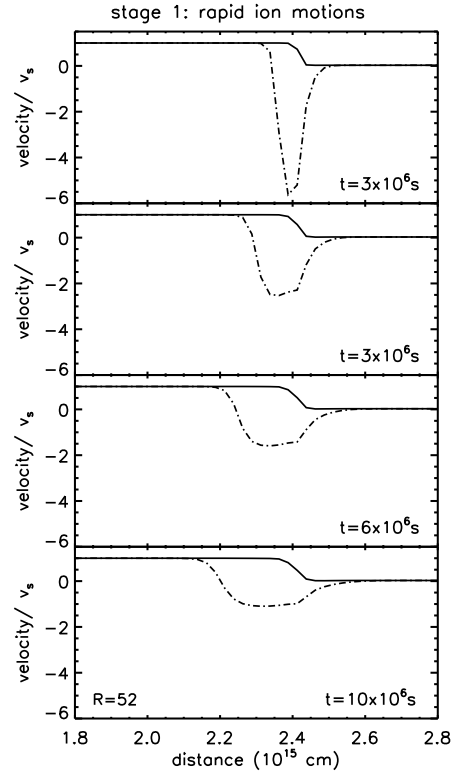


**Fig. 3.** The initial phase in the J to C-shock transition involves rapid ion motions. The neutral (solid line) and ion (dash-dotted line) velocities are shown. Note the distance scale has been expanded, so that the neutral jump shock, spread over 2–3 zones by numerical viscosity, appears rather broad.

### 3. The evolution from J-shock to C-shock

#### 3.1. The four stages for transverse shocks

We identify four stages in the evolution from a J-shock to a C-shock. Each stage lasts approximately 10 times longer than the previous one.

- Stage 1 involves rapid ion motions. It is characterised by high-speed, ion-magnetosonic wave motions over a short time. During the first  $0.002t_{flow} \sim 10^7$  s, the precursor moves upstream at a speed of order  $1000 \text{ km s}^{-1}$ , the ion-magnetosonic speed. As shown in Fig. 3, the ions move upstream (negative velocities), away from the original shock front, with a speed well above the shock speed. The ion compression wave is separated from the neutral front by an ion expansion wave, as expected in this shock-tube experiment.
- During Stage 2 the ion front and the neutral front separate over a time of  $0.03t_{flow} \sim 2 \cdot 10^8$  s, at intermediate speeds (Fig. 4). The ion precursor develops fully. The neutrals possess a weak precursor but are still hardly altered.
- Stage 3 represents the approach to a C-type structure, as the neutrals evolve towards a fully continuous flow. The changes now occur at the Alfvén speed of  $2 \text{ km s}^{-1}$  over a time of  $0.6t_{flow} \sim 4 \cdot 10^9$  s.

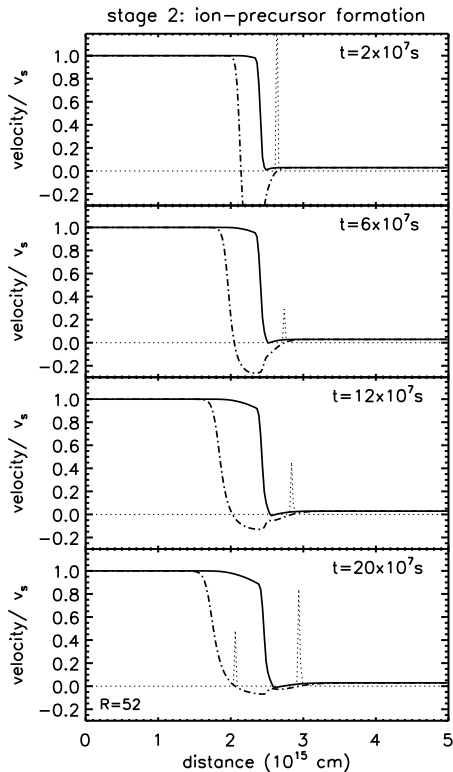


**Fig. 4.** The second phase in the J to C-shock transition. The ion and neutral fronts separate at speeds in the range  $10\text{--}100\text{ km}^{-1}$ . The neutral (solid line) and ion (dash-dotted line) velocities are shown, as well as  $0.001\epsilon_m$  (dotted line), where the momentum error  $\epsilon_m$ , given by Eq. 9, tracks the deviation from the steady-state solution.

- During Stage 4 only small changes to the flow pattern occur. It takes several Alfvén speed crossing times before the steady state solution is finally reached, as described in the previous section (see Fig. 1). The final length scale is  $\sim 1.6\ 10^{15}\text{ cm}$ , approximately equal to  $L_{sm}$ .

### 3.2. Low Alfvén number shocks

Strong magnetic fields cushion a shock by broadening the transition region and reducing the drag heating in the shock front. This is especially important for C-shocks since the cushioning changes the character of the whole transition by reducing the ion-neutral streaming speed whereas for J-shocks it is usually only felt in the downstream compressed gas. Hence we call these C-shocks ‘shock absorbers’ (Smith et al 1991). This cushioning has observational implications: molecules are not so easily destroyed by ion collisions because the ion-neutral streaming speed is a relatively small fraction of the shock speed. In order to model a shock absorber, we simply reduce the shock speed from the standard case by a factor of 10 to simulate a  $M_a = 2.5$  shock.

We find that all the transition stages are identifiable but last several times longer (Fig. 6). Indeed it takes  $\sim 10^4$  years to reach the steady state, comparable to the age of many outflows.

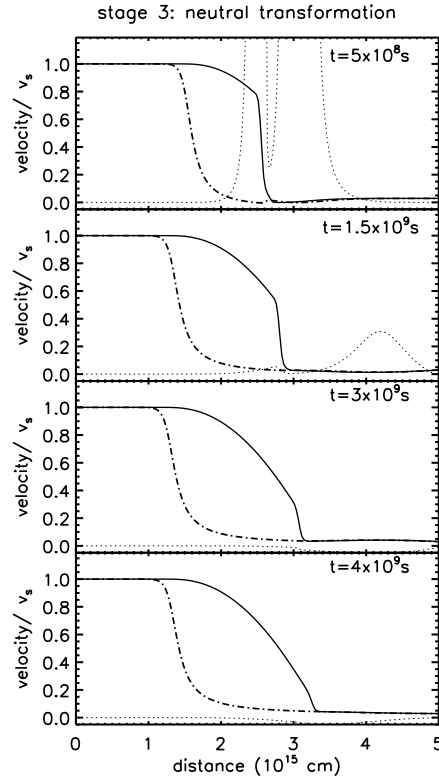


**Fig. 5.** The neutral jump shock finally disappears and the shock width further increases in Stage 3. The neutral (solid line) and ion (dash-dotted line) velocities are shown, as well as  $0.1\epsilon_m$  (dotted line), where the momentum error  $\epsilon_m$  is given by Eq. 9.

Note that the total compression is only about 3 in the example shown. The final total length of the shock is  $\sim 4\ 10^{15}\text{ cm}$ . It is clear that  $L_{sm}$  is indeed an accurate measure of the shock length scale.

### 3.3. Oblique field

Oblique shocks develop from the initial state to a steady-state, oblique C-shock without any surprises. By oblique shock, we specifically mean that the magnetic field is inclined to the shock velocity, but not so far inclined that intermediate shock solutions become possible (Smith 1993c; see below). In this regime, the ion and neutral speeds along the flow direction,  $qv_s$  and  $rv_s$ , behave as before, as shown in Fig. 7. The ion transverse speed  $q_y v_s$  exceeds the neutral transverse speed  $r_y v_s$ . Note also that the ion transverse speed passes through a maximum, and that the shock is narrower than the transverse solution. Thus the grid size was reduced to preserve approximately the same numerical resolution.

### 3.4. Near-parallel field

When the magnetic field is quasi-parallel, the flow does not reduce to the hydrodynamical equivalent, as is often assumed. Even as the transverse field approaches zero, the flow should approach a switch shock solution. This is due to the strong cooling

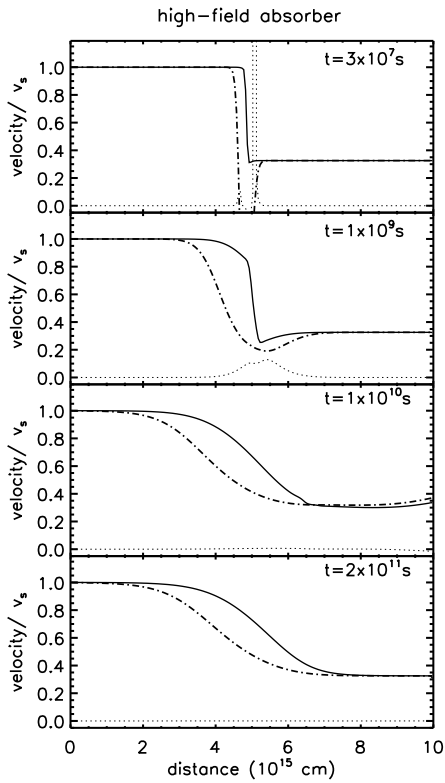


**Fig. 6.** At low Alfvén numbers, the ions and neutrals gently stream against each other. In this model, the shock speed  $v_s = 5 \text{ km s}^{-1}$ , the neutral Alfvén number  $M_a = 2.5$ , the Mach number  $M = 50$ , and the compression  $S = 3.07$ . Note the distance scale has been doubled. The grid size  $R_g = 200$ , so the resolution  $R = 110$  zones in  $L_n$ . The neutral (solid line) and ion (dash-dotted line) velocities are shown, as well as  $0.1\epsilon_m$  (dotted line), where the momentum error  $\epsilon_m$  is given by Eq. 9.

in molecular shocks, or, here, the assumption of isothermality (Smith 1993a,c). Although it is possible that in complex, multi-dimensional, shock configurations a mixture of the three possible shock solutions can be maintained at field angles less than  $\sim 1/M_a$  radians, the switch-type solution is the only evolutionary solution in plane-parallel flows (Kennel 1988).

To compute switch shocks we had to solve several problems. First, we had to set up an appropriate grid. If we take a magnetic field angle of  $2^\circ$  to the flow direction, our standard parameters lead to resolution problems: the neutral shock width is reduced to  $\sim L_n/M_a$ , but, in contrast, the ion precursor extends far upstream. We solve this problem simply by extending the grid upstream using a ratioed grid, and increasing the total number of zones. This problem can still be seen in Fig. 8, where we have reduced  $M_a$  to 5 ( $v_s = 10 \text{ km s}^{-1}$ ). The whole ion precursor, as evident in the upstream transverse ion speed, is still not shown. This precursor will not significantly warm the gas, however, as the heating occurs where the drag is strong and the neutrals decelerate (see Fig. 4. of Smith (1993b)).

A second problem is inherent to the ion treatment in this code: steep ion velocity gradients generate numerical instabilities (Mac Low & Smith 1997b). Unfortunately, such steep gra-

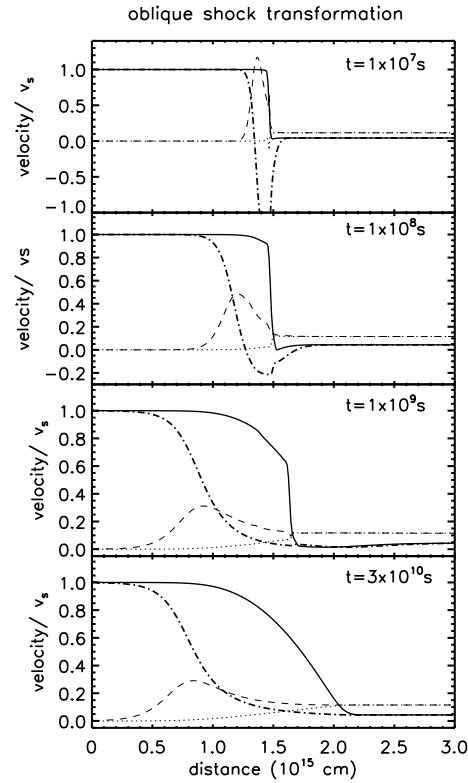


**Fig. 7.** An oblique shock with the upstream magnetic field at an angle of  $30^\circ$  to the shock velocity. The ion (dash-dotted line) and neutral (solid line) velocity components along the flow direction,  $qv_s$  and  $rv_s$ , are shown as before, as well as the transverse speeds  $q_yv_s$  (dashed line) and  $r_yv_s$  (dotted line). The upstream transverse speeds were set to zero. Here  $R_g = 200$ , and  $R = 109$ . The shock speed is  $20 \text{ km s}^{-1}$ , Mach number  $M = 200$  and  $M_a = 10$ , giving a total compression  $S = 23.1$ .

dients are exactly what occurs in flows set up along the field lines. Hence, at early times, up to  $\sim 6 \cdot 10^8 \text{ s}$ , numerical instability is evident within the ion flow. The instability is damped as the gradients diminish. This instability does not occur when, instead of discontinuous initial conditions, we use a hyperbolic tangent function with a width of  $1 \cdot 10^{14} \text{ cm}$ , and we get nearly identical results.

The transverse ion motions are found to have a maximum, as was shown to be true for shocks with  $M_a > 3\sqrt{2}/2$ , in the steady cold solutions of Smith (1993a).

We have also set up the quasi-hydrodynamic, or intermediate Type II boundary and initial jump conditions. In intermediate shocks, the post-shock sound speed is subsonic. As predicted by analytic theory, this flow remained J-type and steady. It is clear that a C-type flow should not occur since the ions, without the inertia of the magnetic field, are now strongly tied to the neutrals. Such Type II J-shocks in multiple dimensions could degenerate into a fast (switch type) and slow shock combination; exactly what is possible depends on the shock configuration and applied conditions (see Smith 1993c). We find, however, that slow shocks (e.g. Smith 1993c) are also restricted to the J-

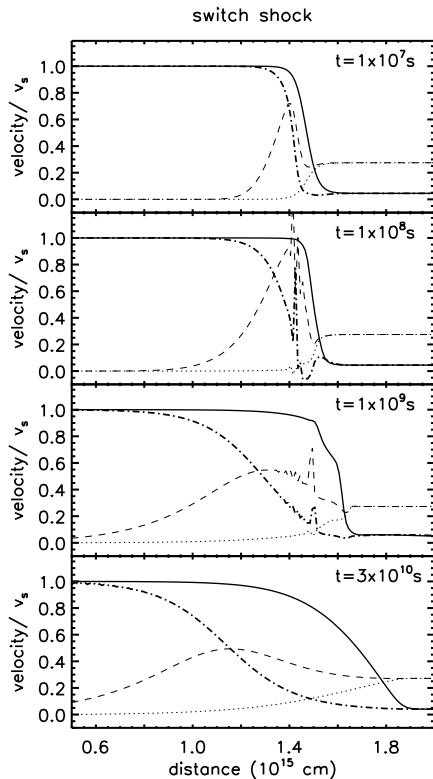


**Fig. 8.** The evolution of a switch shock structure with shock velocity  $v_s = 10 \text{ km s}^{-1}$ , magnetic field at an angle of  $2^\circ$  to  $v_s$ , a compression of  $S = 22.31$ , and  $M_a = 5$ . The parallel field is constant ( $3.43 \cdot 10^{-4} \text{ G}$ ) while the transverse field is ‘switched on’ from  $1.20 \cdot 10^{-6} \text{ G}$  to  $2.37 \cdot 10^{-3} \text{ G}$ . The ion and neutral velocity components are shown as described in Fig. 7. The grid size is  $R_g = 300$  zones, giving a resolution  $R = 121$ .

shock variety. In this case, the sub-Alfvénic motions tie together the ions and neutrals.

Type I intermediate shocks are similar to switch shocks except the small transverse field reverses direction within the shock layer. We find the evolutionary behaviour follows that of the switch shock, but at a slower pace (approximately 3 times slower for the standard conditions with the field initially at  $1^\circ$  to the shock normal.)

We conclude that a continuous range, from C-type to J-type occurs, when the boundary conditions are altered from switch, via Type I and Type II intermediate, to hydrodynamic type. This is emphasized through Fig. 9, which is an example of an intermediate shock close to the I-II transition border. Here the jump shock remains while a partial ion/magnetic precursor develops. Note that here also the transverse ion Alfvén waves propagate far upstream (the complete computational grid is not shown).

### 3.5. Neutralisation in transverse shocks

A class of physical conditions produce another type of shock structure in which the ions are not conserved. A particularly

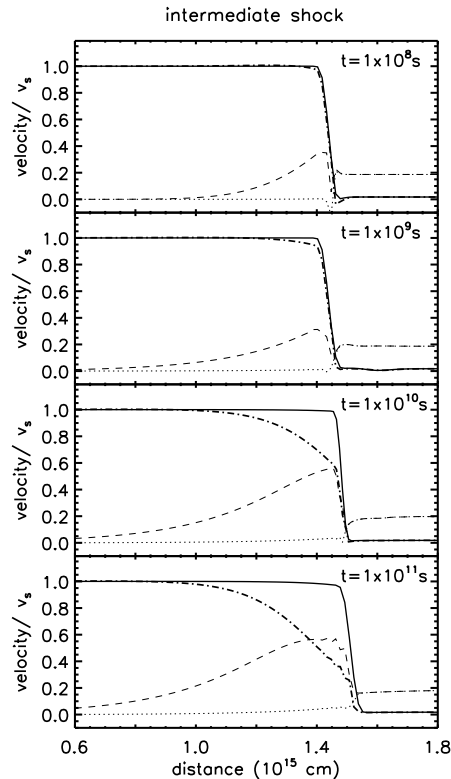


**Fig. 9.** The evolution of an intermediate shock structure with the field at an angle of  $6^\circ$  to the shock velocity, a compression of 57.14, Mach number  $M = 10$ , and neutral Alfvén velocity  $M_a = 5$ . The parallel field is constant ( $0.341 \text{ mG}$ ) while the transverse field flips from  $0.0362 \text{ mG}$  through zero to  $-1.57 \text{ mG}$ . The four lines are as described in Fig. 7, and the grid size is  $R_g = 300$  zones.

simple case, in which the ion fraction remains fixed throughout, is considered here. This can occur when the recombination time is short, such as for molecular ions, with rate coefficients  $R_n \sim 10^{-7} \text{ cm}^3 \text{ s}^{-1}$  rather than atomic ions; and when the shocks are wide enough for neutralisation reactions to occur (Flower et al 1996). Since the shock width is inversely proportional to the ion density, neutralisation is determined solely by the recombination rate coefficient and Alfvén number. The ratio of shock dynamical to recombination times is  $\sim 100(R_n/10^{-7} \text{ cm}^3 \text{ s}^{-1})/M_a$ .

We find that neutralised shocks evolve from the imposed J-type initial state directly to C-type. The neutral jump section is preceded by a ramp of growing amplitude, as shown in Fig. 10. The final C-shock flow pattern is now the ramp structure in the neutrals, preceded by the rapid ion braking. In this zone of rapid ion braking and compression the recombinations will be hard pressed to suppress a rise in ion density. This may lead to a narrow peak in the ion density in reality.

The time to reach steady state in a neutralised shock is much longer than for the other shock types. Almost  $10^4$  years is required for the conditions chosen, comparable with the duration of the Class 0 stage of a protostar. Shock widths are correspondingly larger. Furthermore, the age and shock width are

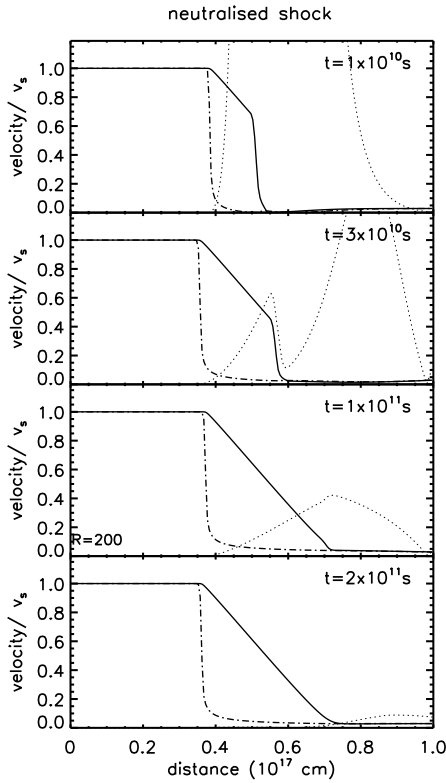


**Fig. 10.** The flow patterns for a neutralised shock transition. All parameters are as chosen for the standard transverse shock except the ion density is held at its initial value. Note the broader shock. The grid size is  $R_g = 200$  zones, so the resolution is only  $R = 68$  zones in the shock width. The neutral (solid line) and ion (dash-dotted line) velocities are shown, as well as the momentum error  $\epsilon_m$  (dotted line).

inversely proportional to the ion density, as we have checked through further simulations. Hence, low-ionisation shocks may never actually reach a steady state.

#### 4. Observables

Shock waves in a magnetized molecular gas will be continuously changing, both through the C-shock instability (Wardle 1990, Neufeld & Stone 1997, Mac Low & Smith 1997a,b) and through interaction with spatial perturbations in density, ion fraction and magnetic field. So how can we recognise the evolving shocks described in this paper? To calculate the emission properties as a function of time, we must first estimate the temperature distribution through the shock. In the continuous sections this can be done using the ‘cool C-shock’ approximation (Smith & Brand 1990a), provided that the temperature remains low so that the thermodynamics and magnetohydrodynamics are decoupled. Quantitatively, we require that the temperature  $T \ll m(\text{H}_2)v_s^2/k$ . The low isothermal temperature adopted ensures this condition in our numerical computations, and strong  $\text{H}_2$  cooling often ensures it in real molecular clouds.

The jump sections are dealt with separately: the jump parameters are transferred into the J-shock code of Smith (1994a),

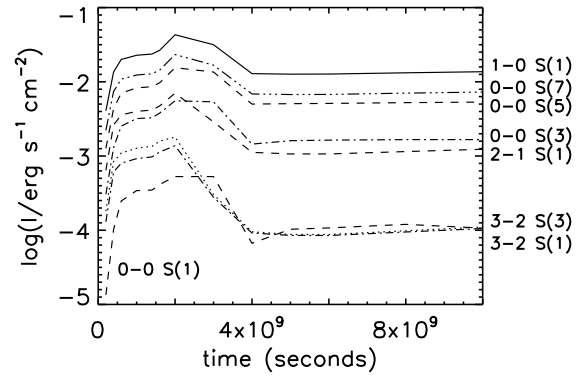


**Fig. 11.** Line intensities versus time for a  $30 \text{ km s}^{-1}$  transverse shock model. The shock is assumed to be observed face on (thus the columns are calculated along a line of sight parallel to the shock velocity). The physical data are given in Table 2.

the column densities in each excited level are calculated, and then added to the column densities derived from the continuous section in the manner described below.

The temperature profile in the continuous section is determined by the local balance of ion-neutral frictional heating with molecular cooling (see Smith 1993b). Simplified cooling functions are adopted consistent with the limitations of the calculations already introduced (in particular the simplified drag formula). Here we restrict the illustrative results to that of  $\text{H}_2$  cooling, with the  $\text{H}_2$  molecule in local thermodynamic equilibrium. The cooling function is extracted from Smith (1993b):

$$\Lambda(T) = (4.2 \cdot 10^{-31} \text{ erg s}^{-1} \text{ cm}^{-3}) n(\text{H}_2) T^{3.3}. \quad (11)$$

It is straightforward to show that the temperature is then given by  $T = 2.89 n_i v_{in}^2$ , where  $v_{in}$  is the ion-neutral streaming speed.

Column densities of molecules in excited upper levels can be computed from

$$N_j = g_j N(\text{H}_2) Z(T) \exp(-T_j/T), \quad (12)$$

assuming that the rotational levels are in LTE at the temperature  $T$ , where the partition function is

$$Z(T) = 0.024 T [1 - \exp(-6000/T)]^{-1}, \quad (13)$$

and  $g_j$  are the statistical weights. Although we assumed the rotational levels are in LTE, we allowed the vibrational levels to fall out of LTE using the method described by Suttner et al. (1997). Line strengths  $I_j$  are then calculated from the column of gas  $N_j(x)$  in the transition’s upper energy level:

$$I_j = \int (hc/\lambda_j) A_j N_j(x) dx, \quad (14)$$

where  $A_j$  is the radiative coefficient and  $\lambda_j$  the wavelength of the transition.

The time dependence of eight lines observable either in the K-band or with the SWS of the Infrared Space Observatory are

**Table 2.** Physical data for selected molecular hydrogen emission lines, observable in either the K-band ( $2\mu\text{m}$ - $2.4\mu\text{m}$ ) or by the SWS of the Infrared Space Observatory (0-0 transitions). Their intensities are plotted in Fig. 11.

Line	$\lambda_j^a$	$T_j^b$	$A_j^c$	$g_j^d$
1-0 S(1)	2.1213	6951.	3.47	21.
3-2 S(3)	2.2008	19086.	5.63	33.
2-1 S(1)	2.2471	12550.	4.98	21.
3-2 S(1)	2.3858	17818.	5.14	21.
0-0 S(7)	5.5110	7199.	2.00	57.
0-0 S(5)	6.9100	4587.	0.588	45.
0-0 S(3)	9.6650	2504.	0.0984	33.
0-0 S(1)	17.0350	1015.	0.00476	21.

<sup>a</sup>Wavelength in  $\mu\text{m}$

<sup>b</sup>Excitation temperature in K

<sup>c</sup>Einstein A-values for radiative deexcitation in  $10^{-7} \text{ s}^{-1}$

<sup>d</sup>Statistical weights with ortho/para ratio of 3

shown in Fig. 11, and the physical parameters of these lines are given in Table 2. The columns of gas are displayed as column density ratios (CDRs) in Fig. 12. A CDR for  $\text{H}_2$  is the column of gas in the energy level  $T_j$  divided by the column of gas in the  $v = 1, J = 3$  level that generates the 1-0 S(1) line, further normalised by the factor  $\exp(T_j/2000\text{K})$  to remove the strong temperature dependence. We thus are comparing column densities to those of a slab of molecular gas at a temperature of 2000 K. These CDR diagrams are an accurate means of displaying the  $\text{H}_2$  excitation over a broad range of energy levels (see also Mac Low & Smith 1997b). A  $30 \text{ km s}^{-1}$  model was chosen for display purposes since this produces gas up to a maximum temperature of  $\sim 2600 \text{ K}$  within the final steady C-shock. The CDRs for a hotter  $40 \text{ km s}^{-1}$  model are also shown. The following stages are recognisable.

- The structure begins as a fast dissociative jump shock with low luminosity in these infrared lines (Fig. 11). The ion-magnetic precursor develops rapidly in the early stages, producing a sharp increase in line strengths.
- The jump speed drops below  $\sim 24 \text{ km s}^{-1}$  at  $\sim 4 \cdot 10^8 \text{ s}$ . Now the molecules survive the jump. The molecules are strongly heated in the jump shock producing a high-excitation spectrum, as best illustrated by the high CDRs during this stage in the high energy levels. Note that HH91A possesses such a high excitation spectra, as shown in Fig. 12.
- The jump weakens and is unable to excite the molecules after  $\sim 3 \cdot 10^9 \text{ s}$ . The shock excitation and line intensities are now controlled by the ion-neutral drag and rapidly approach their final values. The final excitation depends strongly on the shock parameters.

We find no significant variations from the above behaviour for the other types of shocks. Switches, oblique shocks and intermediate shocks are of course hotter than the equivalent transverse shocks. Neutralised shocks possess similar excitation signatures as transverse shocks.

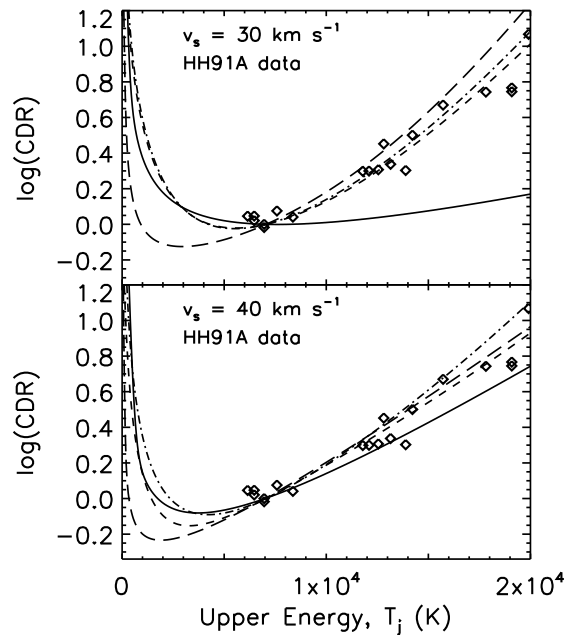


**Fig. 12.** CDR diagrams (see text) for the standard transverse field model with the indicated shock speed and evolution times of  $2 \cdot 10^8 \text{ s}$  (long dash),  $10^9 \text{ s}$  (dot-dash),  $2 \cdot 10^9 \text{ s}$  (dash),  $10^{10} \text{ s}$  (full lines). The data points displayed here were calculated by Smith (1994b) from the intensities observed by Gredel et al (1992). Only positive line detections are shown here.

## 5. Conclusions

We have simulated the evolution of jump shocks into continuous shocks. We set up boundary and initial conditions appropriate to the C-shock, but separated the two flow regimes by a discontinuous diaphragm as in classical shock tube experiments. The questions we hope to answer, however, are more general: how do shocks behave in a non-uniform medium? Do steady-state C-shocks form? We have indeed found that, in all cases, analytic steady-state solutions are approached, given sufficient time. That time can in the most extreme cases, however, be comparable to the lifetimes of embedded protostars.

Four stages were identified for most shock types. First, an ion expansion wave rapidly advances into the upstream region. Next, the ion-magnetic precursor forms and moves gradually upstream, with a high streaming speed capable of heating the molecules. The neutrals develop a weak precursor. Then, the neutral jump weakens and disappears. Finally, the C-shock runs through minor adjustments and reaches the steady state.

In intermediate Type II shocks (which are quasi-hydrodynamic), the full jump shock remains with an ion-precursor in advance. Between Type I and Type II, partial jumps remain. Switch-on shocks develop extremely long ion-magnetic precursors due to forward-moving undamped ionic Alfvén waves. Switch-off shocks, like all slow shocks, are J-shocks.

We have modelled the time-development of molecular hydrogen emission lines in the infrared. If the initial jump shock is

fast, the molecules do not survive, and little emission occurs. As the precursor develops, the line intensities rise rapidly. As the jump shock decreases in strength, the molecules begin to survive and emit with the high excitation characteristic of a jump shock (e.g. with a 1-0 S(1)/2-1 S(1) intensity ratio of 3–5). Later, the jump is too weak to excite H<sub>2</sub> and the C-shock dominates the spectrum, producing line ratios that are very sensitive to the particular parameters of the shock.

The evolution time scale is inversely dependent on the ion density. For typical molecular cloud parameters, it takes between  $(10^9/n_i)$  s and  $(2 \cdot 10^{10}/n_i)$  s to set up the steady-state flow, several times the flow timescale of  $(7 \cdot 10^8/n_i)$  s. Neutralised shocks, modelled here by fixing the ion number density, are approximately  $M_a$  times wider than the transverse equivalent and take the longest to evolve. It follows that detectable changes to the emission lines occur over periods of at least 60 years for the ion density taken here ( $n_i = 0.1 \text{ cm}^{-3}$ ). However, faster evolving shocks, due to high ion densities (perhaps in the densest cloud regions), will show detectable changes faster. The time scale for emission-line variations is  $\sim (2 \cdot 10^8/n_i)$  s where  $n_i$  is the pre-shock ion number density.

This study provides the background to investigations of shock interactions, C-type jet flows, and multi-dimensional studies such as simulations of the Wardle instability (Mac Low & Smith 1997a,b). We hope to add additional physics to this version of ZEUS, including chemical reactions, molecular dissociation and streaming ionisation.

*Acknowledgements.* MDS thanks the DFG for financial support.

## References

- Chernoff, D. F. 1987, ApJ, 312, 143  
 Draine, B. T. 1980, ApJ, 241, 1021  
 Draine, B. T., Roberge, W. G., & Dalgarno, A. 1983, ApJ, 264, 485  
 Draine, B. T., & McKee, C. F. 1993, ARA&A 31, 373  
 Flower, D. R., Pineau des Forets, G., & Hartquist, T.W. 1985, MNRAS, 216, 775  
 Flower, D. R., Pineau des Forets, G., Field, D., & May, P.W. 1996, MNRAS, 280, 447  
 Gredel, R., Reipurth, B., & Heathcote, S. 1992, A&A 266, 439  
 Kaufman, M. J., & Neufeld, D. A. 1996a, ApJ, 456, 250  
 Kaufman, M. J. & Neufeld, D. A. 1996b, ApJ, 456, 611  
 Kennel, C.F. 1988, J. Geophys. Res., 93, 8545.  
 Mac Low, M.-M., Norman, M. L., Königl, A., & Wardle, M. 1995, ApJ, 442, 726  
 Mac Low, M.-M. & Smith, M. D. 1997a, in Low Mass Star Formation— from Infall to Outflow; Poster Proceedings of the IAU Symposium No. 182, eds. F. Malbet and A. Castets (Grenoble, France: Obs. de Grenoble), p. 155  
 Mac Low, M.-M. & Smith, M. D. 1997b, ApJ, submitted  
 Neufeld, D. A. & Stone, J. M., 1997, ApJ, submitted  
 Pineau des Forets, G., in Herbig-Haro Flows and the birth of low mass stars, IAU Symp. No. 182, in press  
 Priest, E., 1982, Solar Magnetohydrodynamics, Reidel, Dordrecht.  
 Roberge, W. G. & Draine, B. T. 1990, ApJ, 350, 700  
 Smith, M. D. & Brand, P. W. J. L. 1990a, MNRAS, 242, 495  
 Smith, M. D. & Brand, P. W. J. L. 1990b, MNRAS, 243, 498

- Smith, M. D. & Brand, P. W. J. L., Moorhouse, A. 1991, MNRAS, 248, 730  
 Smith, M. D. 1991, MNRAS, 253, 175  
 Smith, M. D. 1993a, ApJ, 390, 447  
 Smith, M. D. 1993b, ApJ, 406, 520  
 Smith, M. D. 1993c, A&A, 406, 520  
 Smith, M. D. 1994a, MNRAS, 266 238  
 Smith, M. D. 1994b, MNRAS, 289, 256  
 Smith, M. D. 1995, A&A, 296, 789  
 Stone, J. M. 1997, ApJ, submitted  
 Stone, J. M. & Norman, M. L. 1992a, ApJS, 80, 753  
 Stone, J. M. & Norman, M. L. 1992b, ApJS, 80, 791  
 Stone, J. M. 1992b, ApJs, 80, 791  
 Suttner, G., Smith, M.D., Yorke, H.W., Zinnecker, H., 1997, A&A, 318, 595  
 Tóth, G. 1994, ApJ, 425, 171  
 Tóth, G. 1995, MNRAS, 274, 1002  
 Wardle, M., Draine, B. T. 1987, ApJ, 321, 321  
 Wardle, M. 1990, MNRAS, 246, 98  
 Wardle, M. 1991a, MNRAS, 250, 523  
 Wardle, M. 1991b, MNRAS, 251, 119